https://doi.org/10.5194/amt-2024-8
Preprint. Discussion started: 18 March 2024

Atmospheric Measurement Techniques Discussions

In situ observations of supercooled liquid water clouds over Dome C, Antarctica by balloon-borne sondes

Philippe Ricaud[1], Pierre Durand[2], Paolo Grigioni[3], Massimo Del Guasta[4], Giuseppe Camporeale[5], Axel Roy[1], Jean-Luc Attié[2], and John Bognar[6]

[1]CNRM, Université de Toulouse, Météo-France, CNRS, 42, Avenue G. Coriolis 31057, Toulouse Cedex, France

[2]Laboratoire d'Aérologie, Université de Toulouse, CNRS, UPS, 14 Avenue Edouard Belin, 31400, Toulouse, France

[3]ENEA, Laboratory for Observations and Measurements for Environment and Climate, Via Anguillarese, 301 00123, Rome, Italy

[4]INO-CNR, Via Nello Carrara, 1 – 50019 Sesto Fiorentino, Italy

[5]IREA – CNR, Via G. Amendola n. 122 D/O, 70126 Bari, Italy

[6]Anasphere, Inc., 5400 Frontage Road, 59741Manhattan, MT, USA

Correspondence: philippe.ricaud@meteo.fr

https://doi.org/10.5194/amt-2024-8
Preprint. Discussion started: 18 March 2024

Atmospheric Measurement Techniques Discussions

Abstract

Clouds in Antarctica are key elements that affect radiative forcing and thus Antarctic climate evolution. Although the vast majority of clouds are composed of ice crystals, a non-negligible fraction is constituted of supercooled liquid water (SLW, water held in liquid form below 0°C). Numerical weather prediction models have a great difficulty to forecast SLW clouds over Antarctica favouring ice at the expense of liquid water, and therefore incorrectly estimating the cloud radiative forcing. Remote sensing observations of SLW clouds have been carried out for several years at Concordia station (75°S, 123°E, 3233 m above mean sea level), combining active LIDAR measurements (SLW cloud detection) and passive HAMSTRAD microwave measurements (liquid water path, LWP). The present project aimed at in situ observations of SLW clouds using sondes developed by the company Anasphere, specifically designed for SLW content (SLWC) measurements. These SLWC sondes were coupled to standard meteorological pressure-temperature-humidity sondes from the Vaisala Company and released under meteorological balloons. During the 2021-2022 summer campaign, 15 launches were made, of which 7 were scientifically exploitable. Above a height of 400 m above ground level, we found that the SLWC sondes detected SLW clouds in a vertical range consistent with LIDAR observations. In nominal operation, the LWP values obtained either by HAMSTRAD or vertically-integrated from the SLWC sonde profiles were consistent in spite of their low values (< 10 g m^{-2}). On some occasions far from nominal operation (surface fog, low vertical ascent of the balloon), the LWPs from the SLWC sonde were overestimated by a factor of 5-10 compared to the HAMSTRAD values. In general, the SLW clouds were observed in a layer close to saturation (U > 80%) or saturated (U ~100-105%) just below or at the lowermost part of the entrainment zone or capping inversion zone which exists at the top of the Planetary Boundary Layer and is characterized by an inflection point in the potential temperature vertical

https://doi.org/10.5194/amt-2024-8
Preprint. Discussion started: 18 March 2024

Atmospheric Measurement Techniques Discussions

profiles. Our results are consistent with the theoretical view that SLW clouds form and pertain at the top of the Planetary Boundary Layer.

https://doi.org/10.5194/amt-2024-8
Preprint. Discussion started: 18 March 2024

Atmospheric Measurement Techniques Discussions

1. Introduction

Clouds in Antarctica are key parameters that affect the Earth radiative balance thus the climate evolution over Antarctica but also over the Earth through complex teleconnections (Lubin et al., 1998). The nature of the clouds (ice or liquid or mixed phase, a mixture of liquid and solid water) and their vertical distributions together with their interactions with aerosols add complexity to this topic. Numerical simulations at local or global scales, focused on short time scales or climate evolution show large differences between clouds located above the Southern Ocean, the Western Antarctica – and particularly the Antarctic Peninsula –, the Eastern Antarctic Plateau and in fine Antarctic coastal areas. In general, ice clouds are relatively well estimated by the models while supercooled liquid water (SLW) clouds tend to be underestimated because the water partition function favours solid instead of liquid phase for temperature less than 0°C. This flaw is rather observed in global-scale models but could be reduced in models including a detailed microphysics scheme (e.g. Engdahl et al., 2020). Therefore, the impact of the clouds on the net surface radiation, the so-called cloud radiative forcing, that strongly depends on the nature of the cloud, is usually underestimated by 5-30 W m^{-2} in models that favour ice instead of SLW clouds (King et al., 2006, 2015; Bromwich et al., 2013; Lawson and Gettelman, 2014; Listowski and Land-Cope, 2017; Young et al., 2019). From observations and climate models, it appears that, in Antarctica, the liquid water path (LWP), which is the vertically-integrated SLW content (SLWC), is on average less than 10 g m^{-2}, with slightly larger values in summer than in winter by 2-5 g m^{-2} (Lenaerts et al., 2017), whereas, in the Arctic, values greater than 50 g m^{-2} were reported (Lemus et al., 1997; Zhang et al., 2019) and, at middle/tropical latitudes, values ranging 100-150 g m^{-2} were measured and modelled (Lemus et al., 1997).

In parallel, cloud observations over Antarctica are difficult because of the very small number of ground stations which are located preferably near the coast with only three of them

https://doi.org/10.5194/amt-2024-8
Preprint. Discussion started: 18 March 2024


Atmospheric Measurement Techniques Discussions

opened all year-long deep inside the continent. It is the reason why space-borne measurements are paramount to classify clouds over the entire continent as a function of height, nature, and time. It is clearly accepted now that SLW clouds are much more abundant near the coast than in the inner continent (Bromwich et al., 2012; Listowski et al., 2019) with larger ice crystals and water droplets (Lachlan-Cope, 2010; Lachlan-Cope et al., 2016; Grosvenor et al., 2012; O'Shea et al., 2017; Grazioli et al., 2017) and that the cloud radiative forcing is maximum over the Antarctic Peninsula with values reaching 40 W m^{-2} (Ricaud et al., 2024). In addition to this continent-scale information provided by satellites, it is crucial to obtain information at the local scale from remote and/or in situ observations. Remote observations of SLW/mixed phase cloud are usually performed by means of backscattered LIDARs and ceilometers while in situ observations have been performed over the Southern Ocean (Chubb et al., 2013), Western Antarctica (Grosvenor et al., 2012; Laclan-Cope et al., 2016) and coastal areas (O'Shea et al., 2017) using instruments on board aircraft.

At Concordia station, several studies from remote-sensed observations already took place to evaluate: 1) the presence of the SLW/mixed phase clouds over the station mainly based on a backscattered LIDAR (Cossich et al., 2021), 2) the amount of the LWP within SLW clouds, 3) the impact of SLW clouds on the net surface radiation (Ricaud et al., 2020), 4) the differences between observations and model simulations of SLW clouds, 5) the relationship between in-cloud temperature and LWP, and 6) the relationship between LWP and cloud radiative forcing. In general, SLW clouds are preferably observed in summer with very small LWPs (< 10 g m^{-2}), in-cloud temperatures ranging from -20°C to -38°C and a cloud radiative forcing up to a maximum value of 40 W m^{-2} (Ricaud et al., 2024).

We have thus proposed a new project to observe SLW clouds in situ at Concordia, based on the use of a sonde developed by the Anasphere Company and especially designed for the detection of this type of cloud. During the summer campaign 2021-2022, the SLWC sonde was

https://doi.org/10.5194/amt-2024-8
Preprint. Discussion started: 18 March 2024


Atmospheric Measurement Techniques Discussions

connected to a standard Vaisala pressure-temperature-humidity (PTU) sonde and embarked under an ascending balloon while, during the summer campaign 2022-2023, the two coupled sondes were installed aboard a vertical take-off and landing (VTOL) drone. Numerous SLW clouds were present during the 2021-2022 campaign while, in 2022-23, they were very scarce over the station with a net consequence of measuring only vertical profiles of temperature and relative humidity (Ricaud et al., 2023).

The aim of the present study was to perform for the first time in-situ observations of SLW clouds above the Concordia station during the summer campaign 2021-2022. For the validation and interpretation of the data, we relied on the observations performed by 1) the backscatter LIDAR installed at the station for more than ten years to characterize the nature of the cloud (ice/liquid/mixed phase) and its height and 2) the LWPs measured by the HAMSTRAD radiometer set up at the station in 2009.

The article is structured as follows. The instruments are presented in Sect. 2. The methodology is explained in Sect. 3. The results of the campaign are presented in Sect. 4 before being synthetized and discussed in Sect. 5. A conclusion finalizes the findings in Sect. 6. Note that all the observations performed during the summer campaign are presented in a companion document as supplementary materials.

2. Instruments

In addition to the Vaisala PTU and Anasphere SLW sondes attached to the meteorological balloons, we used observations from two other instruments installed at the Concordia station for several years, namely the backscatter LIDAR to classify the cloud as an SLW cloud, and the HAMSTRAD microwave radiometer to obtain the LWP.

https://doi.org/10.5194/amt-2024-8
Preprint. Discussion started: 18 March 2024

Atmospheric Measurement Techniques Discussions

2.1. PTU sondes

The PTU sondes used during the 2021-2022 summer campaign were standard Vaisala RS-41 SGP sondes (an upgraded version of the Vaisala's RS92 radiosondes), which are now used daily at Concordia to obtain operational temperature and humidity vertical profiles at 12:00 UTC. The sondes were attached to the balloon with a string either unwound before launching (and with a length L = 20 or 40 m) or wound on an unwinder. We systematically used a parachute to obtain vertical profiles in both the ascending and descending phases.

2.2. SLWC sondes

The Anasphere's vibrating-wire sonde records a vibrating wire's frequency as ice accumulates along its length (Serke et al., 2014). These frequency measurements, combined with collocated meteorological measurements, can be used to determine the SLWC of the surrounding air. The SLWC sonde actually measures the frequency of the vibrating wire. Since this frequency f varies according to the change in mass of the wire, its derivative with respect to (wrt) time df/dt can be used to calculate the water collected by the wire, either in the form of ice or absorbed liquid, depending on whether the wire in question is gel-coated or nickel-plated, respectively. From Dexheimer et al. (2019), SLWC (g m^{-3}) is estimated to be:

$$SLWC = -(2b_0 f_0^2 / \varepsilon D \omega f^3) \times (df/dt) \quad (1)$$

where ε is the droplet collection efficiency (~0.9), D is the wire diameter including the hydrophilic gel (0.030 inch or 0.762 mm), b_0 is the vibrating-wire mass per unit length including the hydrophilic gel (2.24 g m^{-1}), ω is the velocity of air relative to the wire (~5 m s^{-1}) and f_0 is the un-iced wire frequency in Hertz ranging from 21.50 to 22.50 Hz during the campaign. f typically ranges from 20.0 to 22.85 Hz during the campaign. The output signal of the sonde is connected to the Vaisala radiosonde which transmits the data to the ground station via telemetry. The observations of the two sondes are thus synchronized. The integration time is 5 s, thus providing an observation every ~25 m along the vertical. We have applied a 4-point

https://doi.org/10.5194/amt-2024-8
Preprint. Discussion started: 18 March 2024


Atmospheric Measurement Techniques Discussions

running average to all our observations. This means that our vertical profiles, even sampled every ~25 m, have a vertical definition of about 100 m. Since it takes about 60-80 s from the launch for the SLWC sonde to stabilize, the minimum height for meaningful observations is ~300-400 m above ground level (agl), below which we are unable to detect any SLW cloud. Note that, in the following, all heights are given in agl.

2.3. LIDAR

The tropospheric depolarization backscatter LIDAR (532 nm) has been operating at Dome C since 2008 (see http://lidarmax.altervista.org/englidar/_Antarctic%20LIDAR.php). The LIDAR provides 5-min tropospheric profiles of aerosols and clouds continuously, from 20 to 7000 m, with a resolution of 7.5 m. LIDAR depolarization (Mishchenko et al., 2000) is a robust indicator of non-spherical shape for randomly oriented cloud particles. A depolarization ratio below 10% is characteristic of SLW clouds, while higher values are produced by ice particles. The potential ambiguity between SLW cloud and oriented ice plates is avoided at Dome C by operating the LIDAR 4° off-zenith (Hogan and Illingworth, 2003).

2.4. HAMSTRAD

HAMSTRAD is a microwave radiometer that profiles water vapour, liquid water and tropospheric temperature above Dome C. Measuring at both 60 GHz (oxygen molecule line (O_2) to derive the temperature) and 183 GHz (H_2O line), this unique, state-of-the-art radiometer was installed on site for the first time in January 2009 (Ricaud et al., 2010). Measurements from the HAMSTRAD radiometer allow the retrieval of vertical profiles of water vapour and temperature from the ground to 10 km altitude with vertical resolutions of 30 to 50 m in the Planetary Boundary Layer (PBL), 100 m in the lower free troposphere and 500 m in the upper troposphere-lower stratosphere. The LWP (g m^{-2}) can also be estimated. The time resolution is adjustable and fixed at 60 seconds since 2018. Note that an automated internal calibration is performed every 12 atmospheric observations and takes about 4 minutes. Consequently, the

https://doi.org/10.5194/amt-2024-8
Preprint. Discussion started: 18 March 2024

atmospheric time sampling is 60 seconds for a sequence of 12 profiles, and a new sequence starts 4 minutes after the end of the previous one. The temporal resolution of the instrument allows the detection of clouds and diamond dust (Ricaud et al., 2017) together with the SLW clouds (Ricaud et al., 2020). The 2021-2022 and the 2022-2023 summer campaigns were dedicated to in-situ observations of SLW clouds using balloons and drone (Ricaud et al., 2023), respectively. Comparisons with numerical weather prediction models showed consistent amounts of LWP at Dome C when the ice-liquid water partition function favours SLW for temperatures below 0°C (Ricaud et al., 2020).

3. Methodology

In order to optimize in-situ SLW cloud observations, we developed the following procedure. 1) The remotely-sensed and real-time observations of clouds (either ice crystals and/or SLW) from the LIDAR were checked regularly. 2) When the presence of SLW was verified, we checked the value of LWP from HAMSTRAD. An empirical value of $LWP_0 = 1.0$ g m^{-2} was estimated as the threshold above which an SLW cloud is considered as significant. For $LWP < LWP_0$, either the amount of liquid water in the cloud was too low or the SLW cloud was too scattered. 3) If the two-above conditions were fulfilled for more than 2 hours, we started the connection and calibration process of the 2 sondes (PTU and SLWC) via the Vaisala Digicora station inside the Concordia station. Then we went outside and inflated the meteorological balloon. Finally, we launched the 2 sondes attached to the balloon using either an unwinder or an unwound string (Figure 1). In total, the step 3) lasted about 1 hour. As we used standard meteorological balloons (Totex TA100), we were able to probe the atmosphere from the surface up to about 12-13 km height (ascent and descent) for a total duration of about 1 hour and 40 minutes. Since the tropopause height was ranging 7-8 km and we were only interested in the first 2 km where the SLW clouds are located, only 2-5% of the observations

https://doi.org/10.5194/amt-2024-8
Preprint. Discussion started: 18 March 2024

made were scientifically sound for our project. This is the main reason why we used a drone during the next campaign 2022-2023 to detect SLW clouds in the PBL (Ricaud et al., 2023). Note that, since there was only one Vaisala Digicora station for both our project and the operational meteorological sounding at 12:00 UTC, we could not use the time window between 09:00 and 14:00 UTC for our studies.

Figure 1: Launch of a Vaisala PTU sonde (left hand of the man in blue) and an Anasphere SLWC sonde (right hand of the man in red) attached to the Totex TA100 meteorological balloon, together with the red parachute and the unwinder for the first flight on 22 December 2021.

In general (see e.g., Ricaud et al., 2020), SLW clouds are usually capped by a thin temperature inversion and a decrease from high relative humidity U (>80%). As this inversion layer separates two layers where temperature decreases with height, it contains an inflection point in the temperature (or potential temperature) profile the height of which $H(T_{inf})$ can be

https://doi.org/10.5194/amt-2024-8
Preprint. Discussion started: 18 March 2024


Atmospheric Measurement Techniques Discussions

used as the top of the atmospheric boundary layer with its capping SLW cloud layer. Such a definition based on the height of the inflection point is frequently used for the determination of the boundary-layer thickness (Hennemuth and Lammert, 2006). Consistent with this definition, Ricaud et al. (2020) adapted from Stull (2012) proposed to consider the potential temperature vertical distribution separating the diurnal variation of the top of the planetary boundary layer into 2 phases: 1) the entrainment zone at the top of the mixed layer where the SLW cloud develops and 2) the capping inversion zone under which the SLW cloud still persists at the top of the residual quasi-mixed layer. The vertical limits of these two layers are well defined by the height of the inflection points $H(\theta_{inf})$. In the following, we have used information from profiles of the potential temperature θ (K) defined as:

$$\theta = T(P_0/P)^{R/C_p} \quad (2)$$

where T is the temperature (K), P the pressure (hPa), P_0 the reference pressure (1000 hPa), R the gas constant of air (J kg^{-1} K^{-1}) and C_p the heat capacity at constant pressure (J kg^{-1} K^{-1}). R/C_p is taken at 0.286. We have characterized inflection points heights $H(\theta_{inf})$ in the potential temperature vertical profiles when the second derivatives in θ with respect to the height z ($d^2\,\theta/dz^2$) are greater than an empirical threshold value typically varying from 1.5 10^{-4} to 4.0 10^{-4} K m^{-2}.

4. Results

4.1. Period of study

The balloon-borne observations of SLW clouds were carried out during the 2021-2022 summer campaign at Concordia. A total of 15 launches were performed from 21 December 2021 to 28 January 2022 (labelled from L01 to L15, respectively). With the exception of 17 January 2022 (L11), when the observations were made to check the behaviour of the SLWC sondes in cloud-free conditions, all other launches were made when a SLW cloud was detected

https://doi.org/10.5194/amt-2024-8
Preprint. Discussion started: 18 March 2024


Atmospheric Measurement Techniques Discussions

for more than 2 hours with the LIDAR observations using the depolarization method described in section 2.3.

Table 1 lists all the launches that were scientifically exploitable in ascending, descending or both modes. In order to avoid listing a catalogue of observations, we chose to only show details and Figures relative to the launches performed on 25 December 2021 and on 17 January 2022 (cloud-free period). Nevertheless, the SLWC vertical distributions calculated for all the flights are shown and discussed in the forthcoming sections. The information regarding all the flights are presented in the supplementary materials. This encompasses: 1) the LWP values from HAMSTRAD and the height range of the SLW clouds from the LIDAR over one day, 2) the profiles of temperature, potential temperature and relative humidity measured by the PTU sonde during the flights, and 3) the profile of the SLWC sonde frequency *f*, the derivative of the frequency wrt time *t* (df/dt) and the calculated SLWC during the flights.

Table 1: List of SLW cloud flights performed during the 2021-2022 season over Concordia, together with date, launch time (UTC) and in italic the time (UTC) when the balloon hits the ground after the descent, SLW cloud vertical range (m) and associated LWP (g m^{-2}) in ascending (ASC) or descending (DES) phase, considering only observations above 400 m agl. Also shown are the SLW cloud vertical range (m) observed by the LIDAR in time coincidence with the flight and the minimum-maximum LWP (g m^{-2}) measured by HAMSTRAD for the same date over 24 hours. Also included are: heights (m) of the inflection point in the vertical profile of potential temperature $H(\theta_{inf})$, information on the type of string used (unwinder or unwound string of length *L*), and any other relevant information (vertical ascent velocity ω less than the nominal 5 m s^{-1}, cloud-free period, surface fog). Heights are always given in meters agl. The root mean square error (RMSE) σ(g m^{-3}) associated with the SLWC profiles in cloud-free conditions is also estimated.

https://doi.org/10.5194/amt-2024-8
Preprint. Discussion started: 18 March 2024

Atmospheric Measurement Techniques Discussions

Launch # ASC/DES	Date YYMMDD	Launch Time HH:MM:SS UTC	Comments	$H(\theta_{inf})$ m	SLW cloud vertical domain		LWP g m^{-2}	
					Sonde m	LIDAR m	Sonde	Hamstrad Min-Max
L01 ASC	211222	02:24:30	Unwinder	710-750	400-500	400-600 750	7.37	2-10
L03 DES	211225	08:53:15 *10:30:00*	Unwinder	950-1000 1450-1500	900-1000 1400-1500	600-800 800-1000 1200-1300	3.67	2-6
L04 ASC	211225	15:48:51	Unwinder	850-880 1400 1520	700-900 1500	700-900	9.08	2-6
L06 ASC	211229	13:45:00	L = 40 m H > 750 m	< 750	750-850	600-800	7.48	1.0-3.5
L07 ASC	211229	17:47:51	L = 40 m ω ~3.5 m s^{-1}	700 850	400-600 750-900	600-800	33.17 23.94	1.0-3.5
L14 ASC	220124	13:51:05	L = 20 m Fog	630 900-920 1400	600 800-1000	800	575.35	1-5
L14 DES	220124	13:51:05 *15:30:00*	L = 20 m Fog	810 1340 1420	800 1000	800	18.92	1-5
L15 ASC	220128	06:08:27	L = 20 m	650 910 1080	600-800 1000-1100	600-800 900-1000	10.15 7.31	2-5
L11 ASC	220117	06:35:15	L = 40 m Cloud Free				~0 σ~0.05 g m^{-3}	0.4-1.0
L11 DES	220117	06:35:15 *08:20:00*	L = 40 m Cloud Free				~0 σ~0.05 g m^{-3}	0.4-1.0

267

268 *4.2. Launches on 25 December 2021*

269 As on 25 December 2021, SLW clouds observed by LIDAR were almost continuously
270 present over Concordia from 00:00 to 19:00 UTC (Figure 2), 2 launches were performed at
271 08:53:15 (L03) and 15:48:51 UTC (L04), from which we will consider both the descending and
272 ascending phases. For 2 hours before the first launch, SLW clouds were observed between 500
273 and 700 m, and during the flight, the SLW clouds were located between 600 and 800 m with
274 some traces of SLW clouds between 1200 and 1300 m, while approximately 2 hours after the
275 flight (when the sondes hit the ground in the descending phase) the SLW clouds were located
276 between 800 and 1000 m. Regarding the second flight, for the 2 hours before the flight, SLW
277 clouds were observed between 700 and 1000 m and, during the flight, around 700-800 m. The
278 first launch was associated with HAMSTRAD-observed LWP of 1.5-6.0 g m^{-2} whereas, for the
279 second flight, it was in the range 1.5-3.0 g m^{-2}. Note that when the sondes reached the ground

https://doi.org/10.5194/amt-2024-8
Preprint. Discussion started: 18 March 2024

Atmospheric Measurement Techniques Discussions

280 at the end of the first launch, the balloon had travelled a distance of about 70 km from the
281 Concordia station after a flight time of 1 h 40 min (Figure 3).

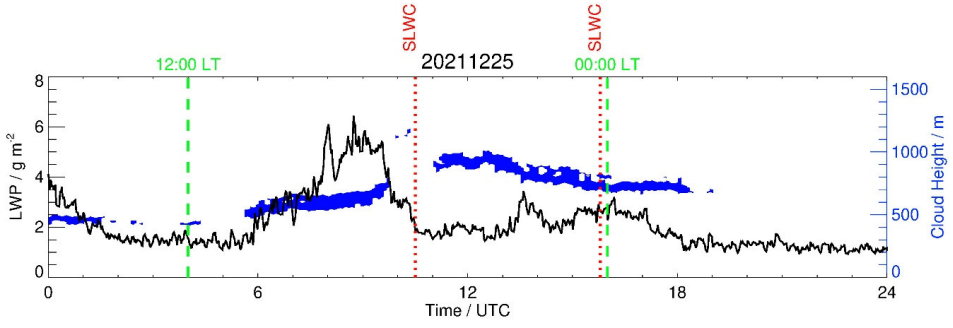

282

283 **Figure 2:** Diurnal variation of the Liquid Water Path (LWP) measured by HAMSTRAD (g m^{-}
284 ^{2}, black solid line) on 25 December 2021 (UTC Time). Superimposed is the SLW cloud
285 thickness (blue area) derived from the LIDAR observations (blue y-axis on the right). Two
286 vertical green dashed lines indicate 12:00 and 00:00 LT. The two red vertical dotted lines
287 indicate the ground landing of the first SLWC sonde (L03 flight) at about 10:30 UTC and the
288 launch of the second SLWC sonde (L04 flight) at about 15:50 UTC, respectively.

289

https://doi.org/10.5194/amt-2024-8
Preprint. Discussion started: 18 March 2024

Atmospheric Measurement Techniques Discussions

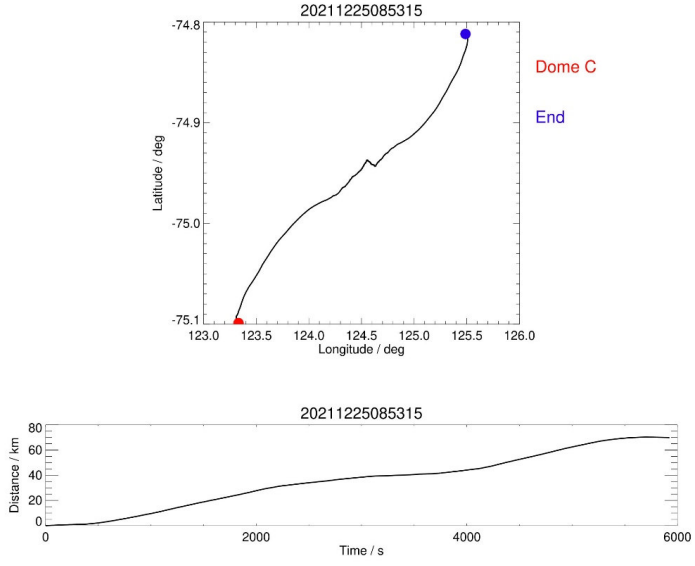

Figure 3: (Top) Path followed by the meteorological balloon launched on 25 December 2021 at 08:53:15 UTC (L03) (red circle) up to the end of the flight (blue circle). (Bottom) Distance travelled (km) as a function of time since launch.

In general, all the flights reached a top height above 10 km (Figure 4 and Figures S7-14), namely well above the tropopause height (about 7-8 km). This is consistent with previous observations made with meteorological operational Vaisala PTU sondes (Tomasi et al., 2015). The profiles of temperature and relative humidity measured during the whole flight (L03) starting at 08:53:15 UTC are shown in Figure 4 together with the calculated potential temperature and observed relative humidity within the layer [400-1600 m]. Above 2 km, a good consistency between ascending and descending phases is found in temperature profiles within ±1 K. The relative humidity profiles are within ±5% of each other, except between 7 and 8.5 km where they differ by around 10%. Below 2 km, the profiles reflect the impact of the PBL. In ascending phase, the heights of inflection points in potential temperature profiles are found at 800-850 m and 1300-1350 m. In descending phase, they are located at 950-1000 m and 1450-

https://doi.org/10.5194/amt-2024-8
Preprint. Discussion started: 18 March 2024


Atmospheric Measurement Techniques Discussions

306 1500 m. Whatever the phase considered, the maximum relative humidity is close to saturation
307 (U ~100%) and can even reach supersaturation by 2 to 5 % (U ~102-105%) in descending
308 phase. This clearly indicates the presence of clouds. Two points need to be underlined. 1) The
309 heights of the potential temperature inflection points are higher by ~150 m in descending
310 compared with ascending phases. The landing occurred 70 km further out and 1 h 40 min later
311 than the launch (Figure 3). This clearly is a fingerprint of both time and space evolution of the
312 PBL top height around the Concordia station. 2) The presence of a set of two distinct inflection
313 points, namely two entrainment zones and/or two capping inversion zones where the SLW
314 clouds develop and/or persist, resemble as if two PBL layers were present above the Concordia
315 station. The explanation could be that the lowest layer is related to the PBL above Concordia
316 although the highest layer is either a remnant of the PBL far from Concordia reaching the station
317 through long-range transport or a fossil layer from the PBL established the day before above
318 the station. These double layers can be clearly identified on 25 December 2021 at 15:48 UTC
319 (Figure 5), on 24 January 2022 at 13:51 UTC (Figure S12) and on 28 January 2022 at 06:08
320 UTC (Figure S13).
321

https://doi.org/10.5194/amt-2024-8
Preprint. Discussion started: 18 March 2024

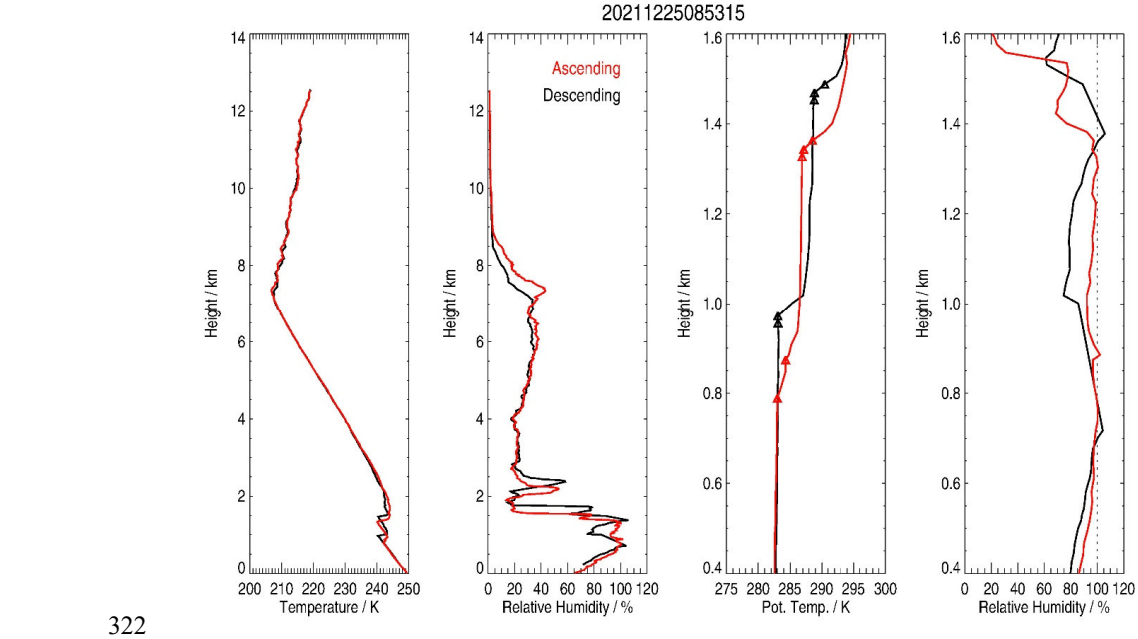

322

323 **Figure 4:** (from left to right) Vertical distributions of: temperature (K), relative humidity (%)
324 observed by the PTU sonde on 25 December 2021 for a launch at 08:53 UTC in ascending (red)
325 and descending (black) phases over the entire vertical range, and potential temperature (K) and
326 relative humidity selected from 400 m to 1600 m height. Red and black triangles in the vertical
327 profiles of potential temperature highlight the presence of inflection points in the ascending and
328 descending phases, respectively. The vertical dotted line in the right panel indicates the 100%
329 relative humidity.

330

https://doi.org/10.5194/amt-2024-8
Preprint. Discussion started: 18 March 2024

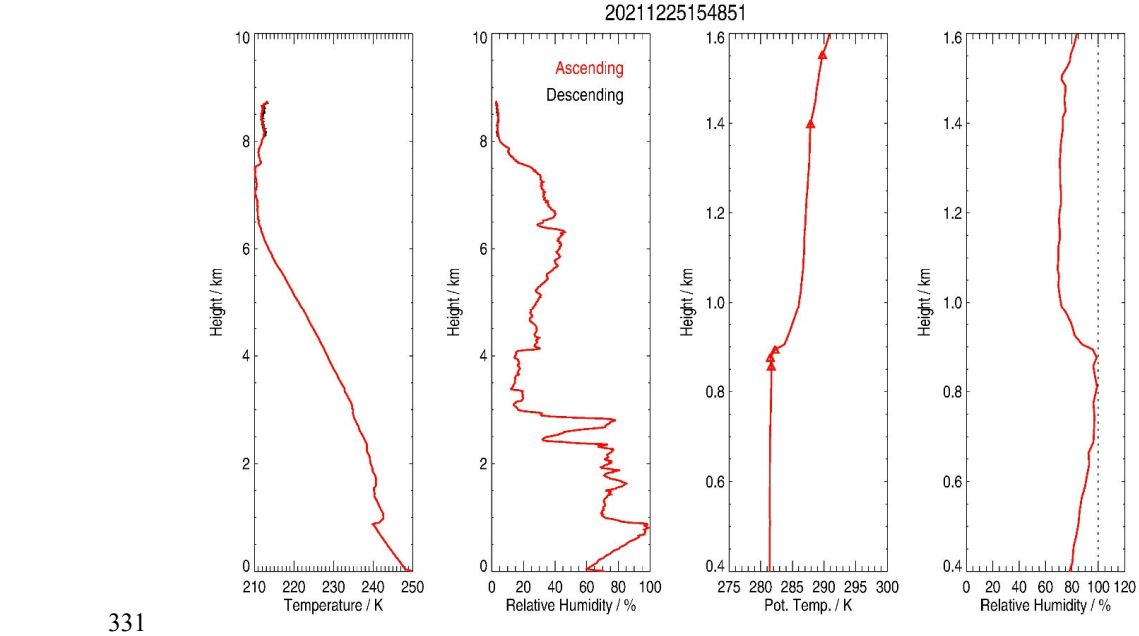

Figure 5: (from left to right) Same as Figure 4 but on 25 December 2021 at 15:48 UTC. Note that, in descending phase (black), only few observations were available after the balloon reached the ceiling height.

The vertical distributions of f, df/dt and SLWC associated with the flights L03 and L04 are shown in Figures 6 and 7, respectively. For both flights, f is rather stable (22.2 and 22.4 Hz, respectively) along the vertical, with a slight increase between 400 and 600 m during L04. For L03, the df/dt values are small (±0.001 Hz s^{-1}) except: 1) between 850 and 1000 m (about -0.005 Hz s^{-1}) where an SLW cloud is estimated from 900 to 1000 m with an SLWC of 0.55 g m^{-3} at 950 m and 2) between 1400 and 1500 m (about -0.001 Hz s^{-1}) where an SLW cloud is estimated from 1400 to 1500 m with an SLWC of 0.25 g m^{-3} at 1400 m, well above the estimated 1-σ random error of 0.05 g m^{-3}. For L04, the df/dt values are small (±0.001 Hz s^{-1}) except: 1) between 700 and 900 m (±0.005 Hz s^{-1}) where an SLW cloud is estimated from 700 to 900 m with an SLWC of 0.35 g m^{-3} at 850 m and 2) around 1500 m (about -0.001 Hz s^{-1}) where an

https://doi.org/10.5194/amt-2024-8
Preprint. Discussion started: 18 March 2024


Atmospheric Measurement Techniques Discussions

346 SLW cloud is estimated around 1500 m with an SLWC of 0.08 g m^{-3}, very close to the estimated
347 1-σ random error of 0.05 g m^{-3}. Note that the df/dt values are high below 500 m, reaching
348 +0.01 Hz s^{-1}, but this is not related to the presence of SLW, which translates as negative values
349 of df/dt (see Equation 1).

350 For L03 (Figure 6), two sets of potential temperature inflection points are measured at
351 $H(\theta_{inf})$ = 950-1000 and 1450-1500 m, with no U measurements at these heights. The SLW
352 clouds derived from the SLWC sonde (900-1000 and 1400-1500 m) are located a within the
353 lowest part of $H(\theta_{inf})$ and few meters below. For L04 (Figure 7), two to three potential
354 temperature inflection points are also measured at $H(\theta_{inf})$ = 850-880, 1400 and 1520 m, with
355 an almost supersaturated atmosphere (U ~100%) at 880 m, and an elevated U ~75% at 1400 m
356 and U ~80% at 1520 m. The SLW clouds derived from the SLWC sonde (700-900 and 1500
357 m) are located within the lowest part of $H(\theta_{inf})$ and few meters below, as for the L03 flight.

358 The SLW cloud heights derived from the SLWC sondes in L03 and L04 are also consistent
359 with the LIDAR observations (600-800, 800-1000 and 1200-1300 m in L03 and 700-900 m in
360 L04). Note that, in L04, the SLW cloud layer derived from the SLWC sonde at 1450 m is not
361 observed by the LIDAR, probably because the underlying SLW cloud at 700-900 m absorbs or
362 reflects most of the LIDAR radiation, which cannot propagate higher. For L03, the vertically-
363 integrated in the 900-1000 m layer of the SLWC calculated from the sonde data is about 3.7 g
364 m^{-2}, which falls within the minimum-maximum LWP values observed by HAMSTRAD on that
365 day (2-6 g m^{-2}) whereas, for L04, the SLWC integrated within the 700-900 m layer is 9.0 g m^{-}
366 ^{2} slightly larger than the minimum-maximum values observed by HAMSTRAD.

https://doi.org/10.5194/amt-2024-8
Preprint. Discussion started: 18 March 2024

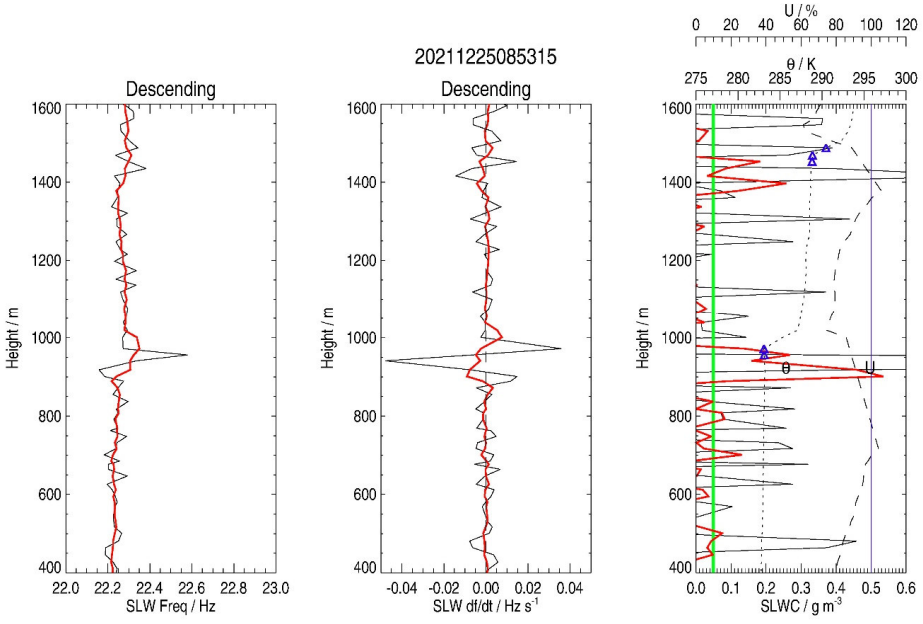

Figure 6: Vertical distribution of: (left) SLWC sonde frequency f (black; Hz), (middle) df/dt (black; Hz s^{-1}); and (right) sonde-calculated SLWC (black; g m^{-3}) on 25 December 2021 at 10:30 UTC (descending phase) for a launch at 08:53:15 UTC. 4-point (20 s) running averages are displayed in red. On the right panel, potential temperature (θ, K) and relative humidity (U, %) are shown as dotted and dashed lines, respectively. Blue triangles represent the height of the potential temperature inflection points. The green vertical line represents the estimated one-sigma error (0.05 g m^{-3}) of the SLWC calculated from the SLWC sonde observations. The blue vertical line indicates the 100% relative humidity.

https://doi.org/10.5194/amt-2024-8
Preprint. Discussion started: 18 March 2024

Atmospheric Measurement Techniques Discussions

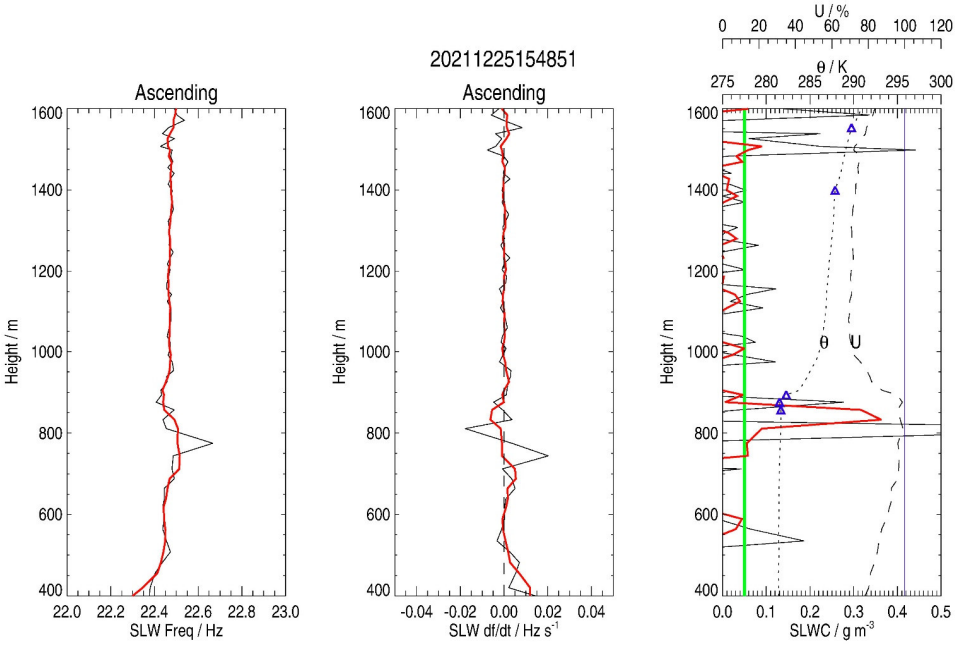

Figure 7: Same as Figure 6, but for 25 December 2021 at 15:48 UTC (ascending phase).

4.3. Launch on 17 January 2022 (cloud-free period)

The launch on 17 January 2022 at 06:15:15 UTC (L11 in ascending and descending phases) was performed in a cloud-free environment throughout the day, as shown by the LIDAR observations (Figures 8), with associated HAMSTRAD-LWP values of 0.4-1.0 g m^{-2}. This launch was an important test to check the behaviour of the SLWC sonde and to quantify the random error associated with the estimation of SLWC. Note that when the sondes reached the ground at the end of the flight, the balloon had travelled a distance of approximately 50 km from the Concordia station after a flight time of 1 h 40 min (Figure 9).

https://doi.org/10.5194/amt-2024-8
Preprint. Discussion started: 18 March 2024

Atmospheric Measurement Techniques Discussions

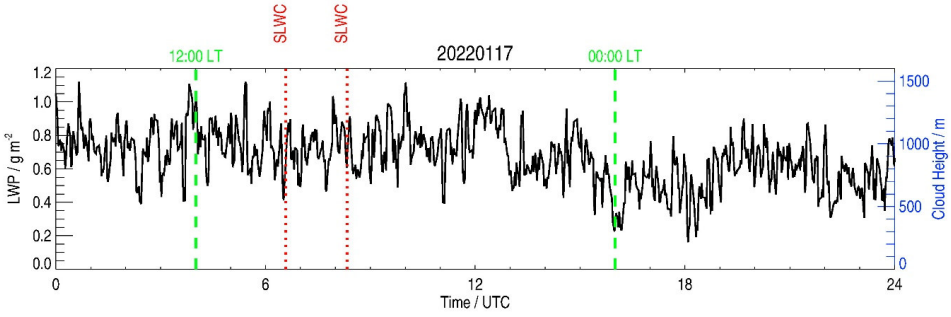

Figure 8: Same as Figure 2, but for 17 January 2022, corresponding to a cloud-free condition period.

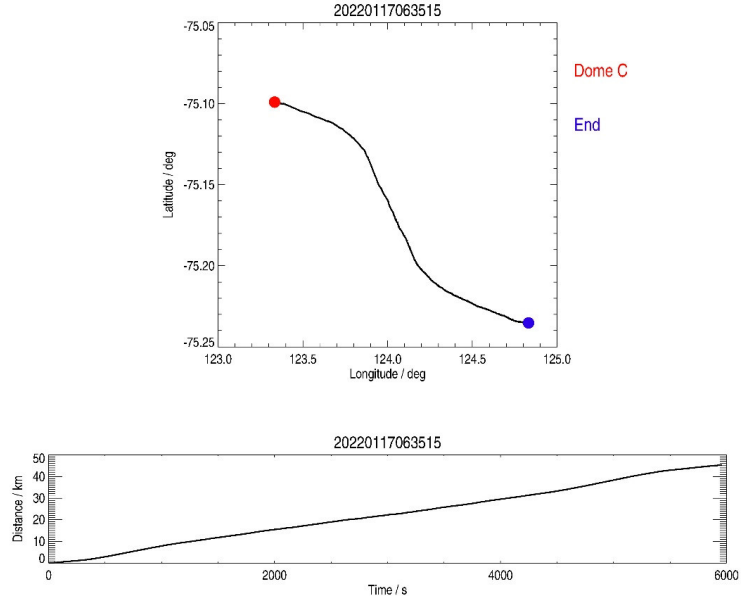

Figure 9: Same as Figure 3, but for the meteorological balloon launched on 17 January 2022 at 07:19:05 UTC.

The profiles of f, df/dt and SLWC for flight L11 in its ascending and descending phases are shown in Figures 10 and 11, respectively. f does not vary much along the vertical in both flight phases with variations lower than ±0.05 Hz producing df/dt values of the order of

https://doi.org/10.5194/amt-2024-8
Preprint. Discussion started: 18 March 2024

Atmospheric Measurement Techniques Discussions

399 ±0.002 Hz s^{-1}. On average, the SLWC oscillates within ±0.05 g m^{-3}. Therefore, we can estimate
400 the random error in the derived SLWC to be σ = 0.05 g m^{-3} and conclude that no SLW clouds
401 were observed with the sonde (although some spikes slightly larger than σ are detected at 400
402 and 1600 m in ascending phase and at 600 and 1200 m in descending phase). This is consistent
403 with the fact that: 1) the relative humidity is low (*U* ranging 10-80%), 2) the LIDAR
404 observations do not show any SLW clouds during the day and 3) the HAMSTRAD LWP is
405 small (<1.0 g m^{-2}).

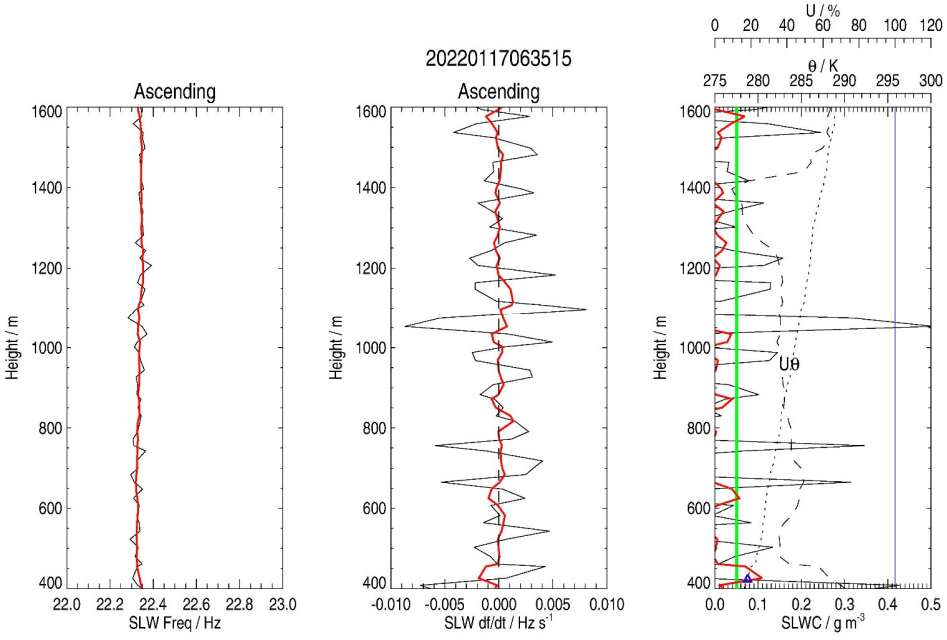

406

407 **Figure 10:** Same as Figure 6, but for 17 January 2022 at 06:35 UTC in ascending phase, in a
408 cloud-free condition.

409

https://doi.org/10.5194/amt-2024-8
Preprint. Discussion started: 18 March 2024

Atmospheric Measurement Techniques Discussions

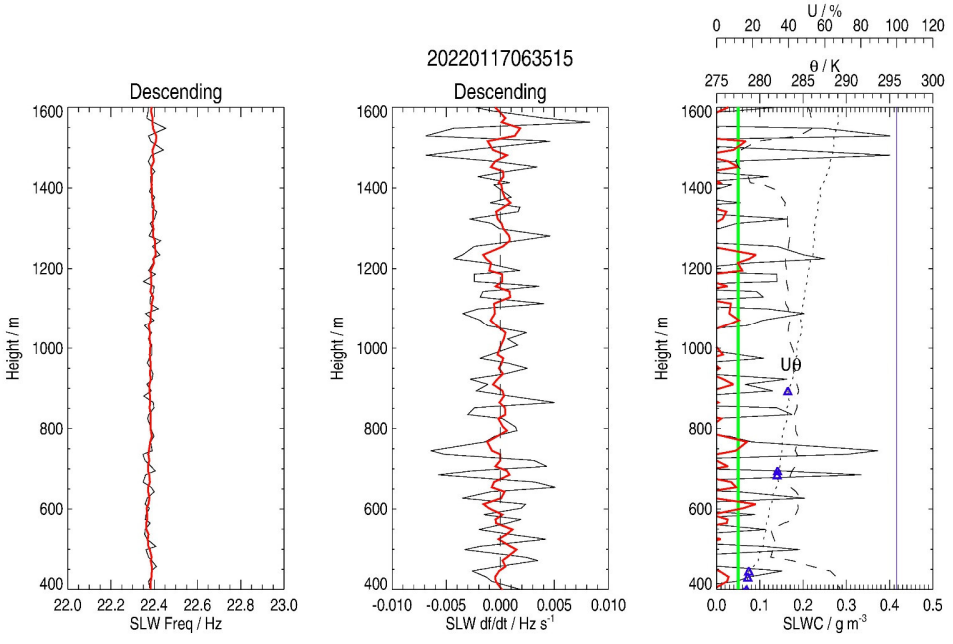

410

411 **Figure 11:** Same as Figure 6, but for 17 January 2022 at 06:35 UTC in descending phase, in a
412 cloud-free condition.

413

414 *4.4. Analysis of all the other flights*

415 The first flight (L01) was carried out on 22 December 2021 at 02:24:30 UTC using an
416 unwinder, after the LIDAR detection of an SLW cloud at 400-600 m between 00:00 and 02:00
417 UTC with an LWP of 8-10.5 g m^{-2} (Figure S1). Unfortunately, just before the launch, the
418 HAMSTRAD-observed LWP decreased to 1.5 g m^{-2}, with some remnants of SLW cloud at 500
419 and 650 m. An SLW cloud is estimated from 400 to 500 m (Figure 12) with an SLWC of 0.35
420 g m^{-3} at 450 m, well above the estimated 1-σ random error of 0.05 g m^{-3}. From 400 to 750 m,
421 U increases from 80 to 90% and $H(\theta_{inf})$ is ranging 710-750 m. The LIDAR observed an SLW
422 cloud at 750 m 20 min after launch slightly higher than the cloud height estimated by the SLWC
423 sonde (400-500 m). The integral into the 400-500 m layer of the SLWC measured by the sonde

https://doi.org/10.5194/amt-2024-8
Preprint. Discussion started: 18 March 2024

Atmospheric Measurement Techniques Discussions

424 is about 7.4 g m^{-2}, which is within the minimum-maximum values observed by HAMSTRAD
425 on that day, namely 2-10 g m^{-2}.

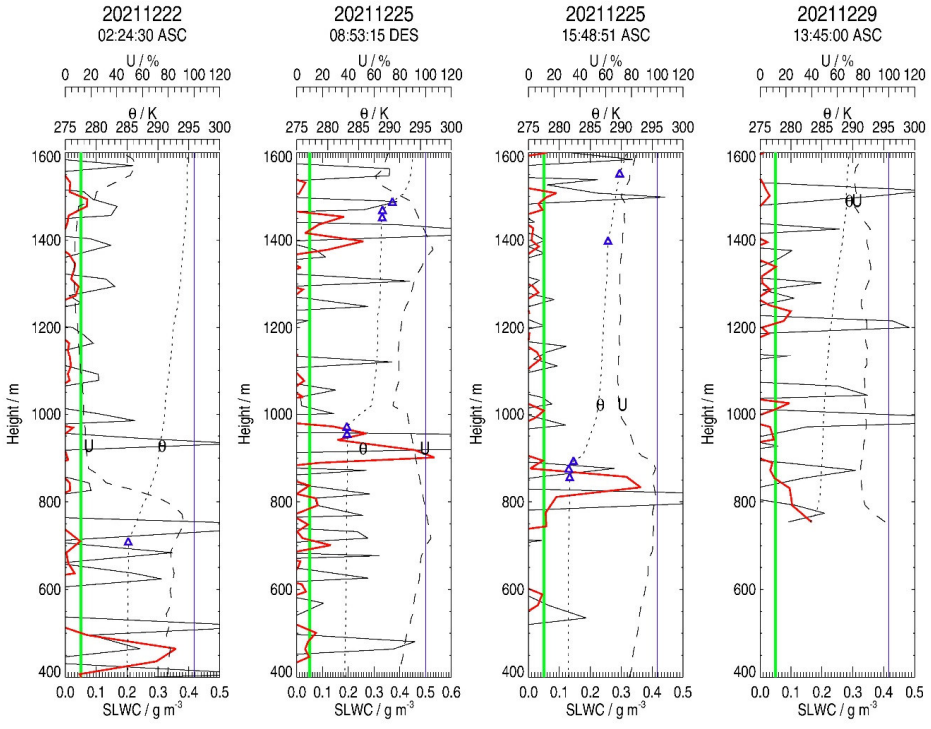

426

427 **Figure 12:** (from left to right) Profiles of SLWC (black; g m^{-3}) observed on: 22 December 2021
428 at 02:24 UTC (ascending phase); 25 December 2021 at 10:30 UTC (descending phase) after a
429 launch at 08:53 UTC; 25 December 2021 at 15:58 UTC (ascending phase) and 29 December
430 2021 at 13:45 UTC (ascending phase). 4-point (20 s) running averages are displayed in red. The
431 potential temperature (θ, K) and the relative humidity (U, %) are shown as dotted and dashed
432 lines, respectively. Blue triangles represent the height of the potential temperature inflection
433 points. The green vertical line represents the estimated one-sigma error (0.05 g m^{-3}) of the
434 SLWC calculated from the SLWC sonde observations. The blue vertical line indicates the 100%
435 relative humidity.

436

https://doi.org/10.5194/amt-2024-8
Preprint. Discussion started: 18 March 2024

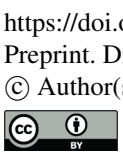

Atmospheric Measurement Techniques Discussions

437 To reduce the duration of instability of the SLWC sonde just after the launch of the balloon,
438 from 29 December 2021, we no longer used an unwinder but an unwound string of length L=40
439 m (L06 and L07 on 29 December 2021 and L11 on 17 January 2022) or L=20 m (L14 on 24
440 January 2022 and L15 on 28 January 2022). We still used a parachute to make observations
441 during the descending phase.

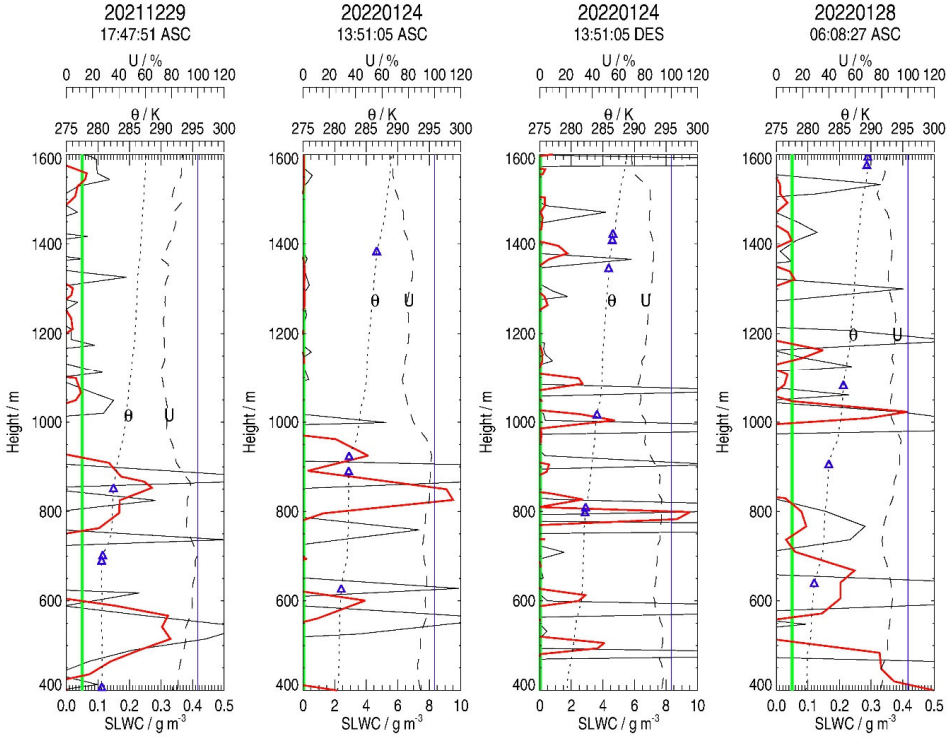

442

443 **Figure 13:** (from left to right) Same as Figure 12 but on: 29 December 2021 at 17:47 UTC
444 (ascending phase); 24 January 2022 at 13:51 UTC (ascending phase); 24 January 2022 at 15:30
445 UTC (descending phase) after a launch at 13:51 UTC and 28 January 2022 at 06:08 UTC
446 (ascending phase).

447

448 On 29 December 2021, two launches occurred at 13:45:00 UTC (L06 in ascending phase)
449 and at 17:47:51 UTC (L07 in ascending phase) after more than 2 hours of SLW clouds observed

https://doi.org/10.5194/amt-2024-8
Preprint. Discussion started: 18 March 2024


Atmospheric Measurement Techniques Discussions

by the LIDAR (Figure S3) between 600 and 800 m, which continued during the flight. The launches were associated with HAMSTRAD-LWP values of 1.5-3.0 g m^{-2}. Note that, on L06, the PTU and SLWC sondes only started acquiring data above 750 m in the ascending phase.

On L06 (Figure 12), an SLW cloud is detected between 750 and 850 m with a maximum of SLWC of 0.16 g m^{-3} and, on L07 (Figure 13), two SLW clouds are estimated, from 400 to 600 m with an SLWC of 0.32 g m^{-3} at 500 m and from 750 to 900 m with an SLWC of 0.28 g m^{-3} at 850 m. On L06, the potential temperature inflection point is certainly below the height when the sondes started acquiring (< 750 m) with near-saturated air at 750 m and, on L07, two potential temperature inflection points are measured at $H(\theta_{inf})$ = 700 and 880 m, with saturated or near saturated air (U ~100% and ~90%, respectively). The SLW clouds derived from the SLWC sonde are in the lowermost part or slightly below $H(\theta_{inf})$. The upper SLW cloud heights inferred from the SLWC sondes in L06 and L07 are also consistent with the LIDAR observations (600-800 m), but the LIDAR does not detect any cloud between 400 and 600 m. The amounts of SLWC observed by the sonde and integrated within the layers 750-850 (L06), 400-600 (L07) and 750-900 m (L07) are about 7.5, 33.2 and 23.9 g m^{-2}, respectively, slightly larger (L06) and much larger (L07) than the minimum-maximum values of the LWP observed by HAMSTRAD on that day (1.0-3.5 g m^{-2}). Two important points need to be emphasised to explain this excess in SLW observed by the sonde on L07. 1) f is not stable along the vertical during the first few hundred meters after launch (Figure S19), contrary to what was observed during the previous flights analysed (sections 4.2 and 4.3). And 2) the ascending velocity on this day was lower (ω ~3.5 m s^{-1}) than the nominal velocity of the air relative to the vibrating wire (~5 m s^{-1}).

On 24 January 2022, we used both the ascending and descending phases of the flight initiated at 13:51:05 UTC (L14) after more than 2 hours of SLW clouds observed by the LIDAR (Figure S4) near the surface between 0 and 200 m. In fact, an episode of intense fog developed

https://doi.org/10.5194/amt-2024-8
Preprint. Discussion started: 18 March 2024


Atmospheric Measurement Techniques Discussions

475 just before the launch. The launch was associated with HAMSTRAD-LWP values of 1.5-3.0 g
476 m^{-2}. One of the main caveats with fog is that, when it is intense, the LIDAR signal cannot
477 propagate efficiently and the presence of a cloud above the fog layer may not be detected. Note
478 that, when the sondes reached the ground at the end of the flight, the balloon had travelled a
479 distance of about 15 km from the Concordia station during 1 h 25 min of flight (Figure S25).
480 In the ascending phase, two SLW clouds are estimated, around 600 m and from 800 to 1000 m
481 (Figure 13). Potential temperature inflection points are detected at $H(\theta_{inf})$ = 630 and 920 m,
482 with air close to saturation (U ~90-95%) and, to a lesser extent, at 1400 m. In the descending
483 phase, several spikes of SLW clouds were detected below 1200 m, but the two most intense
484 were located around 800 and 1000 m (Figure 13). The potential temperature inflection points
485 were measured at $H(\theta_{inf})$ = 800, 1020, 1340 and 1420 m, with relative humidity U ranging 85-
486 95%. In both phases, the SLW clouds derived from the SLWC sonde are located in the
487 lowermost part of the entrainment/capping inversion zone. During the flight, the LIDAR
488 measured two SLW clouds around 350 and 800 m, in addition to near-surface fog. This means
489 that the SLW cloud around 800 m was detected by all the instruments, while an underlying
490 SLW cloud was detected around 600 m by the sondes and much lower (at 350 m) by the LIDAR,
491 slightly below the lowest level where the SLWC sondes start to work well. The SLWCs
492 observed by the sonde and integrated within the layers 800-1000 m (ascending phase) and 750-
493 850 m (descending phase) are about 575.3 and 18.9 g m^{-2}, respectively, much larger than the
494 minimum-maximum values observed by HAMSTRAD on that day (1-5 g m^{-2}). Two important
495 points must be emphasized in order to explain this excess in SLW by the sonde. 1) As far as the
496 flight L14 is concerned, f was not stable along the vertical during the first few hundred meters
497 after launch (Figures S21 and S22), contrary to what was observed during the previous flights
498 analysed (sections 4.2 and 4.3). Above all, the flight was carried out when a fog episode
499 developed over the station. Some ice crystals and/or SLW droplets could well have adhered to

https://doi.org/10.5194/amt-2024-8
Preprint. Discussion started: 18 March 2024

the wire of the SLWC sonde before the launch and perturbed the nominal operation of the sonde system, namely the vibration frequency and the post-launch stabilization process.

The last launch of the summer campaign was performed on 28 January 2022 at 06:08:27 UTC (L15 in ascending phase) after more than 2 hours of SLW clouds observed by the LIDAR (Figure S5) at 600-800 m and 900-1000 m. The launch was associated with HAMSTRAD-LWP values of 3.0-3.5 g m^{-2}. After the launch, the LIDAR detected SLW clouds at about 1000 m. Excluding the large signal at 400 m which is probably due to some residual vibrations from the launch (Figure 13), two SLW clouds are estimated from 600 to 800 m with an SLWC of 0.25 g m^{-3} at 650 m and around 1000 m with an SLWC of 0.40 g m^{-3}. Three potential temperature inflection points are estimated at $H(\theta_{inf})$ = 650, 910 and 1080 m, with U ranging 85-95%. The SLW clouds detected by the SLWC sonde (at 650 and 1000 m) are well within the entrainment/capping inversion zone and at heights consistent with the LIDAR observations (600-800 and 1000 m). The SLWC observed by the sonde and integrated within the 600-800 m and the 950-1050 m layers are about 10.1 and 7.3 g m^{-2}, respectively, slightly larger than the minimum-maximum values observed by HAMSTRAD on that day (2-5 g m^{-2}).

5. Synthesis and Discussion

5.1. SLW cloud

Our study reveals that, during the 2021-22 summer campaign at Concordia, the detection of the SLW cloud heights shows high agreement between the remote sensing observations with the LIDAR and the in-situ observations with the SLWC sondes. The clouds are generally located just below the height $H(\theta_{inf})$ of an inflection point in the potential temperature profile, within a layer where the relative humidity U exceeds 80%, sometimes reaching saturation (100%) and in the lowermost part of the entrainment/capping inversion zone depending on the local time. These results are in agreement both with the theory of the diurnal evolution of the

https://doi.org/10.5194/amt-2024-8
Preprint. Discussion started: 18 March 2024

525 planetary boundary layer (PBL), for which boundary-layer clouds develop at the top of the PBL
526 (Stull, 2012), as well as with the first studies carried out at Concordia based only on remote
527 sensing observations (Ricaud et al., 2020). The presence of the SLW clouds is also observed 1)
528 below the height of the inflection point in potential temperature profile during the High-
529 performance Instrumented Airborne Platform for Environmental Research (HIAPER) Pole-to-
530 Pole Observations global transects over the Southern Ocean (Chubb et al., 2013) and 2) around
531 the height of the inflection point in temperature profile above the South Pole station from
532 backscatter LIDAR signal (Lawson and Gettelman, 2014).

533 The SLWC maxima measured by the sondes were ranging 0.2-0.5 g m^{-3} in nominal
534 operations. This is consistent with: 1) the observations performed in the Arctic with the same
535 sondes and with a surface-based AMF3 microwave radiometer (maxima of 0.3-0.4 g m^{-3})
536 attached to a tethered balloon (Dexheimer et al., 2019), 2) in situ airborne observations from
537 HIAPPER (maximum of 0.47 g m^{-3}) (Chubb et al., 2013), 3) the 580-s observations from the
538 Southern Ocean Clouds, Radiation, Aerosol Transport Experimental Study (SOCRATES)
539 airborne campaign over the Southern Ocean (maximum of SLWCs of 0.60 g m^{-3}) and 4) results
540 from three climate models (maxima of SLWCs ranging from 0.36 to 0.40 g m^{-3}) (Yang et al.,
541 2021).

542 It should also be noted that the variations at scales smaller than 100 m in the vertical
543 profiles of the SLWC observations are smoothed out because of: 1) the 5-s integration time of
544 the raw measurements, 2) the method of deriving the SLWC from equation (1) which requires
545 the use of the vertical derivative of f, and 3) the 4-point running average applied to the
546 observations to minimise the effect of large signal frequency undulations on the retrieved
547 SLWC. Therefore, the actual location of the SLW clouds from the SLWC sondes might be
548 slightly displaced compared with the actual location of the entrainment/capping inversion zone
549 derived from the PTU sondes.

https://doi.org/10.5194/amt-2024-8
Preprint. Discussion started: 18 March 2024


Atmospheric Measurement Techniques Discussions

5.2. Vertically-integrated SLWCs

The vertically-integrated SLWCs calculated from in-situ observations were consistent with the minimum-maximum LWPs observed by HAMSTRAD (flights L01 and L03 with unwinders) or slightly larger than the maximum of LWP (flights L04 and L15 with unwinder and a fixed string of L = 20 m, respectively). Flight L07 (fixed string of L = 40 m) gave a vertically-integrated SLWC greater than that observed by HAMSTRAD by a factor of 5-10, and we can point out that the ascent vertical velocity was certainly too low for the sonde to operate nominally. Finally, for the flight carried out when a fog episode was present (L14), the vibrating wire of the SLWC sonde was probably affected by this event before launch producing an unrealistically large amount of SLWC during the flight. Furthermore, our best results were obtained with an SLWC sonde attached to the balloon with an unwinder.

In nominal operations, LWPs from the sondes were consistent with HAMSTRAD observations (1-14 g m^{-2}). Nevertheless, LWPs observed over Concordia deep inside the Antarctic Plateau were much less than those observed in the Arctic (15-40 g m^{-2} in Dexheimer et al. (2019) and greater than 50 g m^{-2} in Zhang et al. (2019)) and over the coastal Antarctic station of McMurdo (10-50 g m^{-2} in Zhang et al. (2019) and 40-60 g m^{-2} in Hines et al. (2021)).

5.3. Quality/sensitivity of the SLWC sonde

Flying during a cloud-free period helped to characterize the random RMSE σ associated with the retrieved SLWC. Compared to the other flights carried out during the campaign, the cloud-free flight (L11 with a fixed string of L = 40 m) was nominal with a low variability of f during the ascent and descent phases for heights above 400 m, from which we estimated that σ was about 0.05 g m^{-3}.

The way the balloon is released is a key issue for the stability of the SLWC sonde and needs to be addressed whenever the SLW clouds of interest are near the surface within the PBL. Irrespective of the method used (unwinder or unwound string), during the 2021-22 summer

https://doi.org/10.5194/amt-2024-8
Preprint. Discussion started: 18 March 2024

season we were unable to find a way to stabilise the sonde in less than 60 s after launch. One of the main difficulties was that some SLW clouds were located around 400 ± 100 m and, in this case, we were unable to determine whether the variations in the frequency derivatives were due to an instability of the sonde or to a real SLW cloud.

Finally, in our opinion, the optimum way to launch the SLWC sonde was to attach it to the balloon with an unwinder although we obtained one scientifically-exploitable flight using an unwound string of length L=40 m (L07 on 29 December 2021). However, we have only 9 flights and more flights would be needed to confirm this. We have already highlighted the difficulty of numerical weather prediction models to reproduce the SLW clouds over Concordia, which produces erroneous cloud radiative forcings (Ricaud et al., 2020) along with biased temperature and humidity profiles in the PBL (Ricaud et al., 2023). Therefore, in situ observations, although difficult to deploy, still remain a key tool for improving NWPs in these harsh environments.

6. Conclusions

The present study intended to observe in situ SLW clouds above the Concordia station by means of sondes sensitive to SLW especially developed by the Anasphere Company. These sondes were attached to meteorological balloons and connected to standard Vaisala PTU sondes during the 2021-2022 summer campaign. These launches were coupled with observations from a backscattered LIDAR providing the nature and height of the clouds, and a microwave radiometer providing the LWP. Over a total of 15 launches, 7 were scientifically exploitable mainly above 400 m agl, a threshold height imposed by the time the SLWC takes to stabilize after the launch.

In general, during nominal operations, the SLWC sondes detected SLW clouds in a vertical domain consistent with LIDAR observations, and the LWP values either obtained by HAMSTRAD or vertically-integrated from the SLWC values calculated from the sonde

https://doi.org/10.5194/amt-2024-8
Preprint. Discussion started: 18 March 2024


Atmospheric Measurement Techniques Discussions

observations were consistent in spite of their low values (< 10 g m^{-2}). Unfortunately, on some occasions far from nominal operation (surface fog, low vertical ascent of the balloon), the sonde vertically-integrated SLWCs were overestimated by a factor of 5-10 compared to the HAMSTRAD LWPs.

Although the vertical resolution of the SLWC observations is around 100 m due to the methodology employed (4-point running average of 5-s integration time) and the vertical ascent of 5 m s^{-1}, the SLW clouds were observed in a layer close to saturation (U > 80%) or saturated (U ~100-105%) just below or at the lowermost part of the entrainment zone or capping inversion zone which exists at the top of the PBL and is characterized by an inflection point in the potential temperature vertical profiles. Consequently, our results are consistent with the theoretical view that SLW clouds form and pertain at the top of the PBL.

Because of the positive scientific results obtained during this first balloon campaign and since the second campaign in 2022-2023 was technologically successful using a VTOL drone, we forecast a new summer campaign to probe the PBL with an SLWC sonde aboard a drone. The main advantages of the drone compared with the meteorological balloon are that: 1) it can fly every day or even twice a day with the same SLWC sonde onboard minimizing the number of SLWC and PTU sondes used and 2) it does not require Helium gas that is coming to be more and more difficult and costly with time.

Data availability

HAMSTRAD data are available at http://www.cnrm.meteo.fr/spip.php?article961&lang=en (Ricaud, 2024). The tropospheric depolarization LIDAR data are reachable at http://lidarmax.altervista.org/lidar/home.php (Del Guasta, 2024). Radiosondes are available at http://www.climantartide.it/dataaccess/RDS_CONCORDIA/index.php?lang=en (Grigioni, 2024).

https://doi.org/10.5194/amt-2024-8
Preprint. Discussion started: 18 March 2024

625

626 **Author contribution**

627 PR, MDG, GC, AR, PG and JB provided the observational data. PR developed the
628 methodology with the help of all co-authors. All the co-authors participated in the data analysis
629 and in the data interpretation. PR prepared the manuscript with contributions from all co-
630 authors.

631

632 **Competing interests**

633 The authors declare that they have no conflict of interest.

634

635 **Acknowledgements**

636 The present research project Water Budget over Dome C (H2O-DC) has been approved by
637 the Year of Polar Prediction (YOPP) international committee. The permanently staffed
638 Concordia station is jointly operated by Institut polaire français Paul-Emile Victor (IPEV) and
639 the Italian Programma Nazionale Ricerche in Antartide (PNRA). The tropospheric LIDAR
640 operates at Dome C from 2008 within the framework of several Italian national (PNRA)
641 projects. We would like to thank all the winterover personnel who worked at Dome C on the
642 different projects.

643

644 **Financial support**

645 The HAMSTRAD programme 910 and the SLW-CLOUDS programme 1247 were
646 supported by IPEV, the Institut National des Sciences de l'Univers (INSU)/Centre National de
647 la Recherche Scientifique (CNRS), Météo-France, and the Centre National d'Etudes Spatiales
648 (CNES).

649

https://doi.org/10.5194/amt-2024-8
Preprint. Discussion started: 18 March 2024

References

Bromwich, D. H., Nicolas, J. P., Hines, K. M., Kay, J. E., Key, E. L., Lazzara, Lubin, D., McFarquhar, G. M., Gorodetskaya, I. V., Grosvenor, D. P., Lachlan-Cope, T., and van Lipzig, N. P. M.: Tropospheric clouds in Antarctica, Rev. Geophys., 50, RG1004, https://doi.org/10.1029/2011RG000363, 2012.

Bromwich, D. H., Otieno, F. O., Hines, K. M., Manning, K. W., and Shilo, E.: Comprehensive evaluation of polar weather research and forecasting model performance in the Antarctic, J. Geophys. Res.-Atmos., 118, 274–292, 2013.

Chubb, T.H., Jensen, J.B., Siems, S.T. and Manton, M.J.: In situ observations of supercooled liquid clouds over the Southern Ocean during the HIAPER pole-to-pole observation campaigns. *Geophysical Research Letters*, *40*(19), 5280-5285, 2013.

Cossich, W., Maestri, T., Magurno, D., Martinazzo, M., Di Natale, G., Palchetti, L., Bianchini, G., and Del Guasta, M.: Ice and mixed-phase cloud statistics on the Antarctic Plateau, Atmos. Chem. Phys., 21, 13811–13833, https://doi.org/10.5194/acp-21-13811-2021, 2021.

Del Guasta, M.: LIDAR – INO CNR in Antartide, INO-CNR [data set], http://lidarmax.altervista.org/lidar/home.php, last access: 17 January 2024.

Dexheimer, D., M. Airey, E. Roesler, C. Longbottom, K. Nicoll, S. Kneifel, F. Mei, R. G. Harrison, G. Marlton, and P. D. Williams: Evaluation of ARM tethered-balloon system instrumentation for supercooled liquid water and distributed temperature sensing in mixed-phase Arctic clouds, Atmos. Meas. Tech., 12, 6845–6864, https://doi.org/10.5194/amt-12-6845-2019, 2019.

Engdahl, B.J.K., Thompson, G. and Bengtsson, L.: Improving the representation of supercooled liquid water in the HARMONIE-AROME weather forecast model. *Tellus A: Dynamic Meteorology and Oceanography*, *72*(1), 1-18, https://doi.org/10.1080/16000870.2019.1697603, 2020.

https://doi.org/10.5194/amt-2024-8
Preprint. Discussion started: 18 March 2024

675 Grazioli, J., Genthon, C., Boudevillain, B., Duran-Alarcon, C., Del Guasta, M., Madeleine, J.-
676 B., and Berne, A.: Measurements of precipitation in Dumont d'Urville, Adélie Land, East
677 Antarctica, The Cryosphere, 11, 1797–1811, https://doi.org/10.5194/tc-11-1797-2017,
678 2017.
679 Grigioni, P.: Antarctic Meteo-Climatological Observatory, IAMCO [data set],
680 http://www.climantartide.it/dataaccess/RDS_CONCORDIA/index.php?lang=en, last
681 access: 17 January 2024.
682 Grosvenor, D. P., Choularton, T. W., Lachlan-Cope, T., Gallagher, M. W., Crosier, J., Bower,
683 K. N., Ladkin, R. S., and Dorsey, J. R.: In-situ aircraft observations of ice concentrations
684 within clouds over the Antarctic Peninsula and Larsen Ice Shelf, Atmos. Chem. Phys., 12,
685 11275–11294, https://doi.org/10.5194/acp-12-11275-2012, 2012.
686 Hennemuth, B., and Lammert, A.: Determination of the atmospheric boundary layer height
687 from radiosonde and lidar backscatter. *Boundary-Layer Meteorology*, *120*, 181-200,
688 https://doi.org/10.1007/s10546-005-9035-3, 2006.
689 Hines, K.M., Bromwich, D.H., Silber, I., Russell, L.M. and Bai, L.: Predicting Frigid Mixed-
690 Phase Clouds for Pristine Coastal Antarctica. *Journal of Geophysical Research:*
691 *Atmospheres*, *126*(23), p.e2021JD035112, 2021.
692 Hogan, R. J. and Illingworth, A. J.: The effect of specular reflection on spaceborne lidar
693 measurements of ice clouds, Report of the ESA Retrieval algorithm for EarthCARE project,
694 5 pp., 2003.
695 King, J. C., Argentini, S. A., and Anderson, P. S.: Contrasts between the summertime surface
696 energy balance and boundary layer structure at Dome C and Halley stations, Antarctica, J.
697 Geophys. Res.-Atmos., 111, D02105, https://doi.org/10.1029/2005JD006130, 2006.
698 King, J. C., Gadian, A., Kirchgaessner, A., Kuipers Munneke, P., Lachlan-Cope, T. A., Orr, A.,
699 Reijmer, C., Broeke, M. R., van Wessem, J. M., and Weeks, M.: Validation of the

summertime surface energy budget of Larsen C Ice Shelf (Antarctica) as represented in three high-resolution atmospheric models, J. Geophys. Res.-Atmos., 120, 1335–1347, https://doi.org/10.1002/2014JD022604, 2015.

Lachlan-Cope, T.: Antarctic clouds, Polar Res., 29, 150–158, 2010.

Lachlan-Cope, T., Listowski, C., and O'Shea, S.: The microphysics of clouds over the Antarctic Peninsula – Part 1: Observations, Atmos. Chem. Phys., 16, 15605–15617, https://doi.org/10.5194/acp-16-15605-2016, 2016.

Lawson, R. P. and Gettelman, A.: Impact of Antarctic mixed-phase clouds on climate, P. Natl. Acad. Sci. USA, 111, 18156–18161, 2014.

Lemus, L., Rikus, L., Martin, C., and Platt, R.: Global cloud liquid water path simulations. J. Climate, 10(1), 52-64, 1997.

Lenaerts, J. T., Van Tricht, K., Lhermitte, S. and L'Ecuyer, T. S.: Polar clouds and radiation in satellite observations, reanalyses, and climate models, Geophysical Research Letters, 44(7), 3355-3364, 2017.

Listowski, C. and Lachlan-Cope, T.: The microphysics of clouds over the Antarctic Peninsula – Part 2: modelling aspects within Polar WRF, Atmos. Chem. Phys., 17, 10195–10221, https://doi.org/10.5194/acp-17-10195-2017, 2017.

Listowski, C., Delanoë, J., Kirchgaessner, A., Lachlan-Cope, T., and King, J.: Antarctic clouds, supercooled liquid water and mixed phase, investigated with DARDAR: geographical and seasonal variations, Atmos. Chem. Phys., 19, 6771–6808, https://doi.org/10.5194/acp-19-6771-2019, 2019.

Lubin, D., Chen, B., Bromwich, D. H., Somerville, R. C., Lee, W. H., and Hines, K. M.: The Impact of Antarctic Cloud Radiative Properties on a GCM Climate Simulation, J. Climate, 11, 447-462, 1998.

https://doi.org/10.5194/amt-2024-8
Preprint. Discussion started: 18 March 2024

724 Mishchenko, M. I., Hovenier, J. W., and Travis, L. D. (Eds.): Light Scattering by Nonspherical
725 Particles: Theory, Measurements, and Applications, Academic Press, chap. 14, 393–416,
726 2000.
727 O'Shea, S. J., Choularton, T. W., Flynn, M., Bower, K. N., Gallagher, M., Crosier, J., Williams,
728 P., Crawford, I., Flem- ing, Z. L., Listowski, C., Kirchgaessner, A., Ladkin, R. S., and
729 Lachlan-Cope, T.: In situ measurements of cloud microphysics and aerosol over coastal
730 Antarctica during the MAC campaign, Atmos. Chem. Phys., 17, 13049–13070,
731 https://doi.org/10.5194/acp-17-13049-2017, 2017.
732 Ricaud, P.: HAMSTRAD, CNRM [data set],
733 http://www.cnrm.meteo.fr/spip.php?article961&lang=en, last access: 17 January 2024.
734 Ricaud, P., Gabard, B., Derrien, S., Chaboureau, J.-P., Rose, T., Mombauer, A. and Czekala,
735 H.: HAMSTRAD-Tropo, A 183-GHz Radiometer Dedicated to Sound Tropospheric Water
736 Vapor Over Concordia Station, Antarctica, IEEE T. Geosci. Remote, 48, 1365–1380, doi:
737 10.1109/TGRS.2009.2029345, 2010.
738 Ricaud, P., Bazile, E., del Guasta, M., Lanconelli, C., Grigioni, P., and Mahjoub, A.: Genesis
739 of diamond dust, ice fog and thick cloud episodes observed and modelled above Dome C,
740 Antarctica, Atmos. Chem. Phys., 17, 5221-5237, https://doi.org/10.5194/acp-17-5221-
741 2017, 2017.
742 Ricaud, P., Del Guasta, M., Bazile, E., Azouz, N., Lupi, A., Durand, P., Attié, J.-L., Veron, D.,
743 Guidard, V., and Grigioni, P.: Supercooled liquid water cloud observed, analysed, and
744 modelled at the top of the planetary boundary layer above Dome C, Antarctica, Atmos.
745 Chem. Phys., 20, 4167–4191, https://doi.org/10.5194/acp-20-4167-2020, 2020.
746 Ricaud, P., Medina, P., Durand, P., Attié, J.L., Bazile, E., Grigioni, P., Guasta, M.D. and Pauly,
747 B.: In Situ VTOL Drone-Borne Observations of Temperature and Relative Humidity over
748 Dome C, Antarctica. Drones, 7(8), 532, https://doi.org/10.3390/drones7080532, 2023.

https://doi.org/10.5194/amt-2024-8
Preprint. Discussion started: 18 March 2024

749 Ricaud, P., Del Guasta, M., Lupi, A., Roehrig, R., Bazile, E., Durand, P., Attié, J.-L., Nicosia,
750 A., and Grigioni, P.: Supercooled liquid water clouds observed over Dome C, Antarctica:
751 temperature sensitivity and cloud radiative forcing, Atmos. Chem. Phys., 24, 613–630,
752 https://doi.org/10.5194/acp-24-613-2024, 2024.
753 Serke, D., E. Hall, J. Bognar, A. Jordan, S. Abdo, K. Baker, T. Seitel, M. Nelson, R. Ware, F.
754 McDonough, and M. Politovich: Supercooled liquid water content profiling case studies
755 with a new vibrating wire sonde compared to a ground-based microwave radiometer,
756 Atmospheric Research, 149, 77–87, http://dx.doi.org/10.1016/j.atmosres.2014.05.026,
757 2014.
758 Stull, R. B.: An introduction to boundary layer meteorology, Vol. 13, Springer Science &
759 Business Media, 2012.
760 Tomasi, C., Petkov, B., Mazzola, M., Ritter, C., di Sarra, A., di Iorio, T., and del Guasta, M.:
761 Seasonal variations of the relative optical air mass function for background aerosol and thin
762 cirrus clouds at Arctic and Antarctic sites, Remote Sensing, 7(6), 7157-7180, 2015.
763 Yang, C. A., Diao, M., Gettelman, A., Zhang, K., Sun, J., McFarquhar, G., and Wu, W.: Ice
764 and supercooled liquid water distributions over the Southern Ocean based on in situ
765 observations and climate model simulations. Journal of Geophysical Research:
766 Atmospheres, 126, e2021JD036045. https://doi. org/10.1029/2021JD036045, 2021.
767 Young, G., Lachlan-Cope, T., O'Shea, S. J., Dearden, C., Listowski, C., Bower, K. N.,
768 Choularton, T. W., and Gallagher, M. W.: Radiative effects of secondary ice enhancement
769 in coastal Antarctic clouds, Geophys. Res. Lett., 46, 2312–2321,
770 https://doi.org/10.1029/2018GL080551, 2019.
771 Zhang, D., Vogelmann, A., Kollias, P., Luke, E., Yang, F., Lubin, D. and Wang, Z.: Comparison
772 of Antarctic and Arctic single-layer stratiform mixed-phase cloud properties using ground-

https://doi.org/10.5194/amt-2024-8
Preprint. Discussion started: 18 March 2024

based remote sensing measurements. *Journal of Geophysical Research: Atmospheres*, *124*(17-18), 10186-10204, https://doi.org/10.1029/2019JD030673, 2019.